Analysis and modeling of buoyancy generated turbulence using numerical data

Sharath S. Girimaji*

Institute for Computer Applications in Science and Engineering,

NASA Langley Research Center, Hampton, VA 23681

and

S. Balachandar

Department of Theoretical and Applied Mathematics,

University of Illinois, Urbana, IL 61801

ABSTRACT

Rayleigh-Bernard convection offers a unique flow situation in which buoyancy-generated turbulence can be studied in isolation, free of the complicating influence of shear production of turbulence. The objective of this paper is to examine and model important aspects of buoyancy-generated turbulence using direct numerical simulation (DNS) data of Rayleigh-Bernard convection. In particular, we examine the pressure-strain and pressure temperature-gradient correlations, turbulent transport of Reynolds stress, and assumptions pertaining to algebraic modeling of thermal flux and Reynolds stress.

*This research was supported by the National Aeronautics and Space Administration under NASA Contract No. NAS1-19480 while the first author was in residence at the Institute for Computer Applications in Science and Engineering (ICASE), NASA Langley Research Center, Hampton, VA 23681-0001.

1 Introduction

Buoyancy generated turbulence plays an important role in the dynamics of atmospheric boundary layers and engineering applications such as space heating and cooling, electronic equipment cooling and solar collectors. While shear-generated turbulence (mechanical turbulence) has been studied extensively leading to the development of reasonably reliable engineering tools (turbulence models), buoyancy-generated turbulence is relatively less scrutinized [1]. Many of the engineering calculations of thermally dominated flows typically employ empirical correlations involving non-dimensional parameters such as Nusselt, Grashoff and Rayleigh numbers. These empirical correlations lack generality and are usually useful only in situations for which they have been calibrated. Therefore, in buoyant turbulent flows, there is certainly a need for turbulence models that are based on governing equations of the flow and hence possess a reasonable degree of generality. Accurate modeling of buoyancy generated turbulence requires, at least, a working knowledge and understanding of that process. Data gathered from laboratory experiments are usually limited to integral quantities such as heat and mass transfer coefficients. While these quantities are very useful for ultimately validating the models, they lack sufficient detail to shed light on the physics of buoyant turbulence. Direct numerical simulation (DNS), a calculation wherein all of the time and length scales of turbulence are resolved, can provide data with the required degree of detail to study the physics of buoyancy generated turbulence. Although DNS is usually restricted to simple geometry and modest Reynolds numbers, it captures important universal aspects of the physics and has led to the development of some reasonable models of shear-generated turbulence. It is only recently that DNS data has been used in the development of buoyant turbulence models. Dol, Hanjalic and Kenjeres [2] and Girimaji and Hanjalic [3] have used DNS turbulent natural convection data of Boudjemadi *et al.* [4] and Versteegh *et al.* [5] to study certain modeling assumptions and ultimately validate the models. The turbulent convection in this case is between two parallel vertical plates at different temperatures and this configuration gives rise to shear as well as buoyancy generated turbulence.

Our objective in this paper is, using DNS data, to study the Reynolds stress and turbulent thermal flux in a flow where buoyancy is the only source of turbulence production. The turbulent flow in the present case is the Rayleigh-Bernard convection between two horizontal parallel plates at different temperatures. The lower plate is hotter than the upper plate leading to unstable stratification. The turbulence is statistically homogeneous along horizontal planes. The mean velocity is zero everywhere and, hence, there is no shear production of turbulence. Rayleigh-Bernard convection offers a unique flow situation in which buoyancy-generated turbulence can be studied in isolation, free from the complicating influence of shear-generated turbulence. The four specific objectives of this paper are to: (i) to evaluate the pressure-strain and pressure-temperature gradient correlation models using DNS data; (ii) to study the turbulent transport of Reynolds stress and thermal flux; (iii) to examine the various modeling assumptions made to derive algebraic stress models; and, (iv) to develop fully explicit algebraic models for Reynolds stress and thermal flux.

The paper is organized as follows. In Section 2, the governing equations of Reynolds stress and turbulent thermal flux are presented along with their standard closure models. Algebraic models for the Reynolds stress and thermal flux are also developed. Description of the numerical simulation of turbulent Rayleigh-Bernard convection is given in Section 3. We use the simulation data to evaluate and develop various closure models in the Reynolds stress and turbulent thermal flux evolution equations in Section 4. Also in Section 4, we examine the validity of the various assumptions made in the algebraic stress methodology. We conclude in Section 5 with a brief discussion.

2 Governing equations and model development

The buoyant turbulent flow considered here is governed by the usual conservation of mass (continuity), momentum (Navier-Stokes) and temperature (energy) equations subject to the Boussinesq approximation. The flow variables are decomposed into their mean (upper case symbols) and fluctuating (lower case symbols) parts and the equations are Reynolds averaged (averaging is indicated by angular brackets). The resulting Reynolds-averaged Navier Stokes equations are given in most standard text books

and are not presented here. These averaged equations contain two unclosed terms, the Reynolds stress ($\langle u_i u_j \rangle$) and the turbulent thermal flux ($\langle u_i \theta \rangle$).

2.1 Transport equations for $\langle u_i u_j \rangle$ and $\langle u_i \theta \rangle$.

The transport equation for Reynolds stress in a buoyant turbulent flow (with no mean velocity gradients) is given by (Peeters and Henkes [6])

$$\frac{\partial \langle u_i u_j \rangle}{\partial t} + U_k \langle u_i u_j \rangle_{,k} = G_{ij} - \varepsilon_{ij} + \phi_{ij} + \mathcal{D}_{ij}, \tag{1}$$

where the subscript $,k$ indicates differentiation in the k direction. The terms, respectively, are the time rate of change, advection, buoyant production (G_{ij}), dissipation (ε_{ij}), pressure-strain correlation (ϕ_{ij}) and total turbulent diffusion ($\mathcal{D}_{ij}$) of Reynolds stress:

$$\begin{aligned} G_{ij} &= -\beta[\langle u_i \theta \rangle g_j + \langle u_j \theta \rangle g_i] \\ \varepsilon_{ij} &= 2\nu \langle u_{i,k} u_{j,k} \rangle \\ \phi_{ij} &= \langle \frac{p}{\rho_0}(u_{i,j} + u_{j,i}) \rangle \\ \mathcal{D}_{ij} &= [-\langle \frac{p}{\rho_0} u_i \rangle \delta_{jk} - \langle \frac{p}{\rho_0} u_j \rangle \delta_{ik} - \langle u_i u_j u_k \rangle + \nu \langle u_i u_j \rangle_{,k}]_{,k}. \end{aligned} \tag{2}$$

The acceleration due to gravity is given by g_i, ν is kinematic viscosity of the fluid, and ρ_0 is the reference density of the fluid. The buoyant production and dissipation rate of turbulent kinetic energy ($K = \frac{1}{2}\langle u_i u_i \rangle$) are, respectively, $G = \frac{1}{2} G_{ii}$ and $\varepsilon = \frac{1}{2}\varepsilon_{ii}$. The dissipation rate tensor can be split into its isotropic and anisotropic deviatoric parts as follows:

$$\varepsilon_{ij} = \frac{2}{3}\varepsilon \delta_{ij} + d_{ij}. \tag{3}$$

Citing small scale isotropy, the anisotropy of dissipation is generally neglected. The pressure-strain correlation is usually modeled as [6]

$$\phi_{ij} = -C_1 \varepsilon (\frac{\langle u_i u_j \rangle}{2K} - \frac{1}{3}\delta_{ij}) + C_5 \beta (\langle u_i \theta \rangle g_j + \langle u_j \theta \rangle g_i - \frac{2}{3}\langle u_k \theta \rangle g_k \delta_{ij}), \tag{4}$$

where C_1 (usually chosen value lies between 3 and 5) and C_5 (in the range 0.33 to 0.6) are numerical constants. In shear-generated turbulence, the pressure-strain correlation model will also be a function of the mean flow strain rate and vorticity tensors.

The evolution equation of the thermal flux is

$$\frac{\partial \langle u_i \theta \rangle}{\partial t} + U_k \langle u_i \theta \rangle_{,k} = P_{i\theta} + G_{i\theta} + \phi_{i\theta} + \mathcal{D}_{i\theta} - \varepsilon_{i\theta} \tag{5}$$

The terms in the equation correspond to: the time rate of change, advection, thermal production ($P_{i\theta}$), buoyancy production ($G_{i\theta}$), pressure-temperature-gradient correlation ($\phi_{i\theta}$), total turbulent diffusion ($\mathcal{D}_{i\theta}$) and viscous dissipation ($\varepsilon_{i\theta}$):

$$\begin{aligned} P_{i\theta} &= -\langle u_i u_k \rangle T_{,k}; \quad G_{i\theta} = -\beta g_i \langle \theta^2 \rangle; \\ \phi_{i\theta} &= \langle \frac{p}{\rho_0} \theta_{,i} \rangle; \quad \varepsilon_{i\theta} = (\nu + \kappa) \langle u_{i,k} \theta_{,k} \rangle \\ \mathcal{D}_{i\theta} &= [-\langle \frac{p}{\rho_0} \theta \rangle \delta_{ik} - \langle u_i \theta u_k \rangle + \nu \langle \theta u_{i,k} \rangle + \kappa \langle u_i \theta_{,k} \rangle]_{,k}. \end{aligned} \tag{6}$$

The thermal diffusivity of the fluid is κ. The pressure-temperature correlation (in the absence of mean flow velocity gradients) is usually modeled as [6]

$$\phi_{i\theta} = -C_{1\theta} \frac{\varepsilon}{K} \langle u_i \theta \rangle + C_{3\theta} (\beta g_i \langle \theta^2 \rangle). \tag{7}$$

The value of the constant $C_{1\theta}$ in most models range from 3 to 5 and $C_{3\theta}$ is between 0.33 and 0.5. The viscous dissipation ($\varepsilon_{i\theta}$) of thermal flux also needs to be modeled. In sufficiently high Reynolds number flows, the small scales are approximately isotropic leading to $\varepsilon_{i\theta}$ being zero. At lower Reynolds numbers, especially near the walls, viscous dissipation of thermal flux may be non-zero and is modeled as [1]

$$\varepsilon_{i\theta} = f_{\varepsilon\theta} \sqrt{\varepsilon \varepsilon_\theta} \frac{\langle u_i \theta \rangle}{\sqrt{K \langle \theta^2 \rangle}}, \tag{8}$$

where $f_{\varepsilon\theta}$ is a function of the turbulent Peclet number and goes to zero at sufficiently high Reynolds number. The viscous dissipation rate of temperature variance is given by $\varepsilon_\theta = \kappa \langle \theta_{,k} \theta_{,k} \rangle$.

2.2 Algebraic modeling of $\langle u_i u_j \rangle$ and $\langle u_i \theta \rangle$

Often, for calculating practical flows, it is computationally too expensive to solve six differential equations for the Reynolds stress and three more for thermal flux. A more viable approach is the two-equation level of turbulence modeling. At this level of turbulence modeling, the mean fields, turbulent kinetic energy, scalar variance and dissipation rate are obtained by solving their respective evolution equations. Closure is achieved by modeling Reynolds stress and thermal flux with algebraic expressions in terms of the known quantities. We now seek to formulate algebraic models for the anisotropy of Reynolds stress and the correlation coefficient between velocity and temperature fluctuations. We will ultimately verify the validity of the modeling assumptions using simulation data.

The anisotropy of the Reynolds stress is defined as

$$b_{ij} = \frac{\langle u_i u_j \rangle}{2K} - \frac{1}{3}\delta_{ij}, \tag{9}$$

so that

$$\langle u_i u_j \rangle = 2K b_{ij} + \frac{2}{3} K \delta_{ij}. \tag{10}$$

The correlation coefficient between the thermal and velocity fluctuations is defined as

$$F_i = \frac{\langle \theta u_i \rangle}{\sqrt{K}\sqrt{\langle \theta^2 \rangle}}. \tag{11}$$

It is easily seen that the Reynolds stress and thermal flux can be calculated once b_{ij}, F_i, K and $\langle \theta^2 \rangle$ are known.

The governing equations of turbulent kinetic energy and temperature variance are

$$\frac{dK}{dt} = G - \varepsilon + \mathcal{D}_K \tag{12}$$

and,

$$\frac{d\langle \theta^2 \rangle}{dt} = 2(P_\theta - \varepsilon_\theta) + \mathcal{D}_\theta, \tag{13}$$

where the substantial derivative $d/dt = \partial/\partial t + U_j \langle . \rangle, j$. In the above equations, the production of temperature variance is given by

$$P_\theta = -\langle u_i \theta \rangle T_{,i} \tag{14}$$

and, $\mathcal{D}_K = \frac{1}{2}\mathcal{D}_{ii}$ and $\mathcal{D}_\theta = (\kappa\langle\theta^2\rangle_{,kk} - \langle u_k\theta^2\rangle_{,k})$ are the total turbulent transport of kinetic energy and temperature variance respectively.

2.3 Transport equations for b_{ij} and F_i.

The rate of change of the anisotropy tensor and thermal flux correlation coefficient can be evaluated using chain rule

$$\frac{db_{ij}}{dt} = \frac{1}{2K}\frac{d\langle u_i u_j\rangle}{dt} - \frac{\langle u_i u_j\rangle}{2K^2}\frac{dK}{dt}; \tag{15}$$

and,

$$\frac{dF_i}{dt} = \frac{1}{\sqrt{K\langle\theta^2\rangle}}\frac{d\langle\theta u_i\rangle}{dt} - \frac{1}{2}F_i[\frac{1}{K}\frac{dK}{dt} + \frac{1}{\langle\theta^2\rangle}\frac{d\langle\theta^2\rangle}{dt}]. \tag{16}$$

Since we are dealing with normalized quantities, it is best to consider the evolution equations in normalized time. The turbulent velocity and thermal timescales can be defined respectively as

$$\tau_v = \frac{K}{\varepsilon}; \quad \tau_\theta = \frac{\langle\theta^2\rangle}{\varepsilon_\theta}. \tag{17}$$

The overall timescale (τ) of the buoyant process is taken to be the geometric mean of the individual timescales:

$$\tau = \sqrt{\tau_v\tau_\theta}. \tag{18}$$

Time increment in normalized time is given by $dt^* = dt/\tau$.

The evolution equation of the anisotropy tensor can be easily derived by substituting equations (1), (4) and (12) into equation (15). In normalized time, the evolution equation is

$$\begin{aligned}
\frac{db_{ij}}{dt^*} &= -\frac{1}{2}(F_i g_j^* + F_j g_i^* - \frac{2}{3}F_k g_k^*\delta_{ij}) - \frac{1}{2}C_1\frac{\tau\varepsilon}{K}b_{ij} \\
&\quad + \frac{C_5}{2}(F_i g_j^* + F_j g_i^* - \frac{2}{3}F_k g_k^*\delta_{ij}) + (F_k g_k^* + \frac{\tau\varepsilon}{K})b_{ij} \\
&\quad \tau[\frac{1}{2K}\mathcal{D}_{ij} - \frac{\langle u_i u_j\rangle}{2K^2}\mathcal{D}_K] + \frac{\tau}{2K}d_{ij} \\
&= [\frac{\tau\varepsilon}{K}(1 - \frac{C_1}{2}) + F_k g_k^*]b_{ij} + \frac{C_5 - 1}{2}(F_i g_j^* + F_j g_i^* - \frac{2}{3}F_k g_k^*\delta_{ij}) \\
&\quad \tau[\frac{1}{2K}\mathcal{D}_{ij} - \frac{\langle u_i u_j\rangle}{2K^2}\mathcal{D}_K] + \frac{\tau}{2K}d_{ij}.
\end{aligned} \tag{19}$$

The following normalizations have been used:

$$T_j^* = \tau\sqrt{\frac{K}{\langle\theta^2\rangle}}T_{,j}; \quad g_i^* = \beta\sqrt{\frac{\langle\theta^2\rangle}{K}}\tau g_i. \tag{20}$$

The transport equation for the thermal flux correlation coefficient is derived by substituting equations (5), (7), (8), (12) and (13) into equation (16):

$$\begin{aligned}\frac{dF_i}{dt^*} &= -2(b_{ij}+\frac{1}{3}\delta_{ij})T_j^* - \eta g_i^* - \\ &F_i(C_{1\theta}\frac{\tau}{\tau_v}+f_{\varepsilon\theta}) - \frac{1}{2}F_i[\sqrt{\frac{\tau_\theta}{\tau_v}}(\frac{G}{\varepsilon}-1)+2\sqrt{\frac{\tau_v}{\tau_\theta}}(\frac{P_\theta}{\varepsilon_\theta}-1)] \\ &\tau[\frac{\mathcal{D}_{i\theta}}{\sqrt{K\langle\theta^2\rangle}} - \frac{1}{2}F_i(\frac{\mathcal{D}_K}{K}+\frac{\mathcal{D}_\theta}{\langle\theta^2\rangle})],\end{aligned} \tag{21}$$

We can simplify the various production to dissipation ratios as follows:

$$\begin{aligned}\frac{1}{2}\sqrt{\frac{\tau_\theta}{\tau_v}}\,[\frac{G}{\varepsilon}] &= \frac{1}{2}\sqrt{\frac{\tau_\theta}{\tau_v}}\,[\frac{-\beta g_i\langle\theta u_i\rangle}{\varepsilon}] = -\frac{1}{2}g_i^*F_i, \\ \sqrt{\frac{\tau_v}{\tau_\theta}}\,[\frac{P_\theta}{\varepsilon_\theta}] &= \sqrt{\frac{\tau_v}{\tau_\theta}}\,[\frac{-\langle u_i\theta\rangle T_{,i}}{\varepsilon_\theta}] = -F_iT_i^*.\end{aligned} \tag{22}$$

Weak equilibrium assumption. In slowly evolving flows, the mean quantities (T_i^* and g_i^*) evolve more slowly in space and time than the turbulence quantities (b_{ij} and F_i). The turbulence quantities, in normalized time, quickly settle down to equilibrium values on the imposition of mean flow parameters. The weak-equilibrium assumption states that the turbulence is approximately in equilibrium with the imposed mean flow parameters. This equilibrium state of the turbulence can be obtained by setting the substantial derivative of the turbulence quantities to zero:

$$\frac{db_{ij}}{dt^*} = \frac{dF_i}{dt^*} = 0. \tag{23}$$

Further, in the weak-equilibrium limit we assume that the turbulent transport of anisotropy tensor and the thermal flux correlation coefficient are negligible. This is equivalent to the following models for turbulent transport:

$$\begin{aligned}\mathcal{D}_{ij} &= \frac{\langle u_iu_j\rangle}{K}\mathcal{D}_K \\ \mathcal{D}_{i\theta} &= F_i[\frac{1}{2}\sqrt{K\langle\theta^2\rangle}(\frac{\mathcal{D}_K}{K}+\frac{\mathcal{D}_\theta}{\langle\theta^2\rangle})].\end{aligned} \tag{24}$$

2.4 Algebraic model for b_{ij}.

The transport equation (19) for the anisotropy of Reynolds stress, on invoking the weak-equilibrium assumptions (equations 23 and 24) yields

$$b_{ij} = \frac{C_5 - 1}{\frac{\tau\varepsilon}{K}(C_1 - 2) - 2F_k g_k^*}(F_i g_j^* + F_j g_i^* - \frac{2}{3}F_k g_k^* \delta_{ij}). \tag{25}$$

This is the algebraic model for the anisotropy of Reynolds stress in buoyancy dominated turbulent flows. The anisotropy is a function of the normalized gravity and thermal flux vectors and the constants in the pressure strain-correlation model.

2.5 Algebraic model for F_i.

Invoking the approximations in equations (23) and (24), we obtain from equation (21)

$$F_i = -\frac{1}{Q}[2b_{ij}T_j^* + \frac{2}{3}T_i^* + \eta g_i^*], \tag{26}$$

where $\eta = 1 - C_{3\theta}$ and

$$Q \equiv \frac{1}{2}[\sqrt{\frac{\tau_\theta}{\tau_v}}(\frac{G}{\varepsilon} - 1) + 2\sqrt{\frac{\tau_v}{\tau_\theta}}(\frac{P_\theta}{\varepsilon_\theta} - 1)] + C_{1\theta}\frac{\tau}{\tau_v} + f_{\varepsilon\theta i}. \tag{27}$$

Using equation (22), we can write

$$Q = -F_i(T_i^* + \frac{1}{2}g_i^*) + Q_0 \tag{28}$$

where

$$Q_0 = \sqrt{\frac{\tau_\theta}{\tau_v}}(C_{1\theta} - \frac{1}{2}) - \sqrt{\frac{\tau_v}{\tau_\theta}} + f_{\varepsilon\theta}. \tag{29}$$

The expression given in equation (26) is not yet a model for F_i since the thermal flux appears on the right hand side of the equation also (in Q). The modeling will be complete only if Q can be expressed in terms of known quantities.

Determination of Q. The quantity Q must be such that the model for F_i is self-consistent. Multiplying either side of equation (26) by $(T_i^* + \frac{1}{2}g_i^*)$ we obtain:

$$F_i(T_i^* + \frac{1}{2}g_i^*) = -\frac{1}{Q}(\eta g_i^* + \frac{2}{3}T_i^* + 2b_{ij}T_j^*)(T_i^* + \frac{1}{2}g_i^*), \tag{30}$$

which can be restated using equation (28) as

$$Q(Q_0 - Q) = -(\eta g_i^* + \frac{2}{3}T_i^* + 2b_{ij}T_j^*)(T_i^* + \frac{1}{2}g_i^*), \tag{31}$$

We need to solve this equation to obtain Q. Such a value of Q will lead to a self-consistent model for F_i.

Define the following invariants:

$$I_1 = g_i^*(T_i^* + \frac{1}{2}g_i^*); \quad I_2 = T_i^*(T_i^* + \frac{1}{2}g_i^*); \quad I_3 = b_{ij}T_j^*(T_i^* + \frac{1}{2}g_i^*). \tag{32}$$

Substitution of (32) into equation (31) leads to a quadratic equation for Q:

$$Q^2 - Q_0 Q - I_0 = 0, \tag{33}$$

where

$$I_0 \equiv \eta I_1 + \frac{2}{3}I_2 + 2I_3. \tag{34}$$

Therefore,

$$Q = \frac{1}{2}[Q_0 \pm \sqrt{Q_0^2 + 4I_0}]. \tag{35}$$

Clearly Q has to be real. Therefore, it is very important that the pressure-temperature gradient correlation model coefficients are such that the discriminant is always positive.

In the context of Rayleigh-Benard convection considered here, the nondimensional mean thermal gradient, T_i^*, exists only along the vertical direction ($T_1^* = T_2^* = 0$ and $T_3^* \neq 0$). At large Rayleigh numbers, and correspondingly large Reynolds numbers, this normalized vertical gradient of mean temperature is large and negative and confined to thin thermal boundary layers near the top and bottom boundaries. In the interior, away from the boundaries, $T_3^* \approx 0$. The nondimensional gravity vector g_3^*

is also negative since it points opposite to the vertical z direction. The negativity of both T_3^* and g_3^* guarantees that in Rayleigh-Bernard convection I_1, I_2 and I_3 are each individually positive leading to I_0 being positive over the entire convective layer. As a result, the discriminant, $Q_0^2 + 4I_0$, is always positive. In the interior I_0 can be approximated as $\frac{\eta}{2}(g_3^*)^2$.

Given that I_0 is positive, it is easy to show that one of the roots is always positive:

$$Q^{(1)} = Q_0 + \sqrt{Q_0^2 + 4I_0} \geq 0. \tag{36}$$

The other root is always negative:

$$Q^{(2)} = Q_0 - \sqrt{Q_0^2 + 4I_0} \leq 0. \tag{37}$$

On inspection of the model for thermal flux (equation 26) it is clear that a positive value of Q leads to a gradient diffusion of thermal flux, whereas a negative value means counter-gradient diffusion. In a homogeneous turbulent convection flow near the 'weak-equilibrium' state, counter-gradient is unphysical. Therefore, we deem that the only physically permissible model for Q is the positive root given in equation (36). Equation (26) in conjunction with (36) is the fully-explicit and self-consistent model for the normalized thermal flux.

3 Numerical simulation of Rayleigh-Bernard turbulence

We consider the classical problem of Rayleigh-Benard convection in a layer of fluid bounded between two horizontal plates. When the bottom plate is maintained sufficiently hotter than the top plate, thermal instability drives the flow and at large enough temperature difference the flow becomes fully turbulent. Since in this configuration the mean velocity is identically zero, turbulence is purely driven by buoyancy and shear generation is absent. A DNS database ([7], [8]) will be used to test the validity of the various modeling assumptions and the effectiveness of algebraic modeling of Reynolds stress and thermal flux terms in this purely buoyancy driven flow.

Numerical simulations were performed in a box of a square platform with height to width aspect ratio of $2\sqrt{2}$. A schematic of the computational geometry along with the coordinates is shown in figure

1. The governing Boussinesq equation along with the incompressibility condition were solved using spectral methods. The top and bottom boundaries were considered to be isothermal, impermeable and stress-free, while the horizontal directions were periodic. One of the nondimensional parameters in this formulation, the Prandtl number, was chosen to be 0.72 corresponding to that of air. The other nondimensional parameter, the Rayleigh number, was chosen to be 6.5×10^6. This Rayleigh number is nearly four orders of magnitude greater than the critical Rayleigh number of 657 and this places present simulation in the hard thermal turbulence regime, according to the classification of Castaing *et al.* [9]. The computations were well resolved with a uniform grid of 96 points along the horizontal directions and 97 points along the vertical direction. Computational data was collected over a long duration of more than 40 eddy turn-over times, defined as $H/K^{1/2}$, where H is the height of the convecting layer of fluid. All of the data presented below are nondimensionalized with a length scale of H, velocity scale of $\sqrt{RaPr/2Nu}(\kappa/H)$ and temperature scale of $\sqrt{4Nu^3/RaPr}\Delta T$, where κ is the thermal diffusivity of the fluid, ΔT is the temperature difference between the top and the bottom boundaries. The Nusselt number, Nu, for the present simulation is about 23. The above proper scaling [10] differs from the conventional diffusional scaling by factors $\sqrt{RaPr/2Nu}$ and $\sqrt{4Nu^3/RaPr}$ in the velocity and temperature scales. The diffusion scaling is well known to result in very large nondimensional velocity at large Rayleigh numbers and the above proper scaling will reduce all nondimensional quantities to order one.

The periodic boundary conditions along the horizontal directions lead to translational invariance and statistical homogeneity along the x and y directions. The presence of top and bottom boundaries introduces inhomogeneity along the vertical direction. As a consequence, single point turbulence statistics are functions of only the vertical direction. Even in the vertical direction approximate homogeneity can be expected in the interior sufficiently away from the top and bottom boundaries. In figure 2, the mean temperature, $< \theta >$, the mean square temperature fluctuation, $< \theta^2 >$ and the turbulent kinetic energy, K, are plotted as a function of the vertical coordinate. It is clear that the rapid variation in the mean temperature is limited to the two thermal boundary layers adjacent to the top and bottom

boundaries and that the mean temperature is nearly uniform in the interior 90% of the convecting layer. Owing to the stress-free boundary conditions, the horizontal components of velocity are non-zero at the top and bottom boundaries, resulting in relatively large kinetic energy at z=0 and 1. Both $< \theta^2 >$ and K are also nearly constant over the interior 50% of the layer.

4 Evaluation of closure models and modeling assumptions

In this Section, we use simulation data to evaluate models and modeling assumptions. Specifically, we investigate the following three important modeling issues: (i) pressure correlation models; (ii) the evolution equation budgets of Reynolds stress anisotropy and normalized thermal flux to evaluate the validity of algebraic stress modeling assumptions; and, (iii) behavior of the turbulent transport terms. Owing to homogeneity along the horizontal directions (x-y plane), the Reynolds stress anisotropy (b_{ij}) and thermal flux correlation coefficient (F_i) are both functions of only the vertical (z) direction. Furthermore, invariance between x and y directions, along with the constraint $b_{ii} = 0$, leads to $b_{11} = b_{22} = -\frac{1}{2}b_{33}$. From symmetry arguments the other off-diagonal terms of the Reynolds stress anisotropy tensor are zero. Similarly, mean thermal flux exists only along the vertical direction and the horizontal components of the thermal flux vector are zero. Therefore, in the following sections we perform the model evaluation on the b_{33} and F_3 components only. Models will be first evaluated with standard commonly used model constants. Using the DNS, optimal values of model coefficients will also be evaluated. Here the optimal value of the model coefficient is that which minimizes the root mean square of the difference between the data and the model.

4.1 Reynolds stress models

Pressure-strain correlation. Away from the walls, the pressure-strain correlation is the most important turbulence process that needs closure modeling. The fact that this phenomenon is present in the simplest of homogeneous flows as well as the most complex has made this one of the most studied turbulent processes in mechanical turbulence. The fluctuating pressure in buoyancy-driven turbulence

can be divided into two parts, each governed by a Poisson equation:

$$\begin{aligned} p^s_{,ii} &= -u_{i,j}u_{j,i} \\ p^f_{,ii} &= \beta g_i \theta_{,i}, \end{aligned} \tag{38}$$

where p^s and p^f are the slow and fast (buoyancy) components of pressure. Along the same lines the pressure strain model is decomposed into the slow and the fast pressure-strain correlation terms. The slow term is also called the return to isotropy term, since on the removal of all turbulence generating mechanism, this term returns the turbulence from an initial anisotropic state to isotropic state.

The most comprehensive pressure-strain correlation model in buoyant turbulence is given by Ristorcelli *et al* [11]. This model is constructed using joint realizability constraints on Reynolds stress and turbulent thermal flux and has the right behavior in rotating flows. The Ristorcelli model is however quite complicated in structure and the model most commonly used in practical applications is as given in equation (4). When appropriately normalized, as they appear in the b_{ij} evolution equation (19), the fast and the slow terms of the model are

$$\begin{aligned} \frac{\tau}{2K}\phi^f_{ij} &= \frac{1}{2}C_5(F_i g^*_j + g^*_i F_j - \frac{2}{3}F_k g^*_k \delta_{ij}) \\ \frac{\tau}{2K}\phi^s_{ij} &= -C_1 \frac{\tau\varepsilon}{2K} b_{ij}, \end{aligned} \tag{39}$$

where C_1 and C_5 are numerical constants. The more general pressure-strain model involves additional constants C_2-C_4 and are typically used with production terms of mechanical origin.

In figure 3, the ϕ^f_{33} component as calculated from DNS data is presented as a function of vertical height z. The standard model with a commonly chosen value of 0.5 for C_5 is also plotted. Clearly, the model reproduces the DNS results very poorly. Even the qualitative trend is not captured by the model. It should be pointed out that the model does not contain any near-wall correction terms and, hence, cannot be expected to do well close to the wall. But in the center region of the flow, the model presents a nearly flat profile, whereas the data clearly indicates a parabolic profile with the maximum at the center. In search of better agreement, we hypothesize an extended fast pressure model of a type

sometimes used in mechanical turbulence:

$$\frac{\tau}{2K}\phi_{ij}^{f} = C_1^* \frac{\tau}{2K} G b_{ij} + \frac{1}{2} C_5 (F_i g_j^* + g_i^* F_j - \frac{2}{3} F_k g_k^* \delta_{ij}), \tag{40}$$

where G is the buoyant production rate. The optimum values for C_1^* and C_5 are determined to be -3.0 and 0.54 respectively. The optimized model is also plotted in figure 3. As can be seen, the agreement away from the walls is very good. The negative value of C_1^* is significant, for it implies that in energetic turbulence the model will remain realizable. This is because, in energetic, turbulence, production is positive and this term has the effect of bringing anisotropy back towards zero which is indeed the function of the pressure strain correlation, to redistribute the kinetic energy equally among the three components. Had the coefficient been positive, the new term would have increased the anisotropy beyond the bounds of realizability in highly energetic turbulence.

The evaluation of the slow-term model is performed in figure 4. The DNS data indicates that the slow-term is very large at the walls and gets progressively smaller, attaining its minimum near the center. The standard model captures the trend qualitatively, but quantitative agreement leaves a lot to be desired. When an optimized value is used for C_1, the agreement improves slightly near the walls at the expense of poorer agreement at the center. An expanded model which included a non-linear term in anisotropy was tried without much improvement in the agreement. This leads us to the conclusion, that the numerical coefficient C_1 should perhaps be a variable depending upon the local state of the turbulence.

Algebraic model verification and budget of b_{ij}. The budget of b_{ij} evolution equation is now investigated to evaluate the validity of the algebraic modeling assumptions. For the weak-equilibrium assumption to be valid we should have negligible rate of change of anisotropy following a fluid particle and negligible turbulent transport of anisotropy so that the balance is between production, dissipation and pressure-strain correlation. The turbulence under consideration here is statistically stationary and has no mean velocity field and hence there is no mean flow advection of anisotropy. Therefore, algebraic modeling assumption will be valid if the turbulent transport of b_{ij} is negligible. Referring to equation

(19), the assumptions can be stated as

$$\mathcal{D}^b_{ij} \approx d^b_{ij} \approx 0; \quad \phi^b_{ij} = -(P^b_{ij} - \varepsilon^b_{ij}), \tag{41}$$

The definitions of these terms can be easily gathered from equation (19):

$$\begin{aligned}
P^b_{ij} &\equiv -\frac{1}{2}[F_i g^*_j + F_j g^*_i - \frac{2}{3}F_k g^*_k \delta_{ij}] + F_k g^*_k b_{ij} \\
\varepsilon^b_{ij} &\equiv -\frac{\tau\varepsilon}{K} b_{ij} \\
\phi^b_{ij} &\equiv -\frac{C_1}{2}\frac{\tau\varepsilon}{K} b_{ij} + \frac{C^*_1}{2} F_k g^*_k b_{ij} + \frac{C_5}{2}[F_i g^*_j + F_j g^*_i - \frac{2}{3}F_k g^*_k \delta_{ij}] \\
\mathcal{D}^b_{ij} &\equiv \tau[\frac{1}{2K}\mathcal{D}_{ij} - \frac{\langle u_i u_j \rangle}{2K^2}\mathcal{D}_K] \\
d^b_{ij} &\equiv \frac{\tau}{2K} d_{ij}.
\end{aligned} \tag{42}$$

In figure 5, ϕ^b_{33}, $-(P^b_{33} - \varepsilon^b_{33})$, $\mathcal{D}^b_{ij}$ and d^b_{ij} are plotted. In order for the algebraic model to be successful it is required that $\phi^b_{33} \approx -(P^b_{33} - \varepsilon^b_{33})$ and the remaining terms be negligible. This is clearly not the case. The turbulent transport of anisotropy, although smaller than the other terms, is not entirely negligible even in the center of the channel. This term is large enough to result in significant differences between the pressure-strain correlation model and $-(P^b_{33} - \varepsilon^b_{33})$. Therefore, we conclude that the algebraic Reynolds stress model (equation 25) may not be appropriate for this flow. The anisotropy of dissipation is also shown in the figure and it is negligible.

Turbulent transport of b_{ij}. The modeling assumption that the turbulent transport of b_{ij} is negligible implies that the anisotropy of turbulent transport is identical to that of the Reynolds stress itself:

$$\mathcal{D}^b_{ij} \approx 0; \quad \frac{\mathcal{D}_{ij}}{2\mathcal{D}} - \frac{1}{3}\delta_{ij} \approx \frac{\langle u_i u_j \rangle}{2K} - \frac{1}{3}\delta_{ij} = b_{ij}. \tag{43}$$

From figure 5, it is clear that such is not the case and, hence, we will now take a closer look at turbulent transport. It can be seen from equation (2) that the turbulent transport can be classified into pressure transport, transport through triple correlation and viscous transport. In figure 6, the three components of $\mathcal{D}^b_{33}$ calculated from the DNS data are shown as a function of the vertical height. While

the viscous transport is reasonably small, the other two are certainly not negligible. The pressure transport is particularly large near the walls and significant even near the center and needs to be carefully accounted for in modeling.

4.2 Thermal flux models

Pressure temperature correlations. The pressure temperature-gradient correlation can again be decomposed into slow and fast parts which are modeled commonly as follows:

$$\begin{aligned} \phi^s_{i\theta} &\equiv \langle \frac{p^s}{\rho_0}\frac{\partial \theta}{\partial x_i}\rangle \approx -C_{1\theta}\frac{\varepsilon}{K}\langle u_i\theta\rangle, \\ \phi^f_{i\theta} &\equiv \langle \frac{p^f}{\rho_0}\frac{\partial \theta}{\partial x_i}\rangle \approx C_{3\theta}(\beta g_i\langle\theta^2\rangle). \end{aligned} \tag{44}$$

Dol and Hanjalic [2] found that the commonly used models were better suited for simulating the temperature pressure-gradient terms. In other words, they propose

$$\begin{aligned} -\langle \frac{\theta}{\rho_0}\frac{\partial p^s}{\partial x_i}\rangle &\approx -C_{1\theta}\frac{\varepsilon}{K}\langle u_i\theta\rangle, \\ -\langle \frac{\theta}{\rho_0}\frac{\partial p^f}{\partial x_i}\rangle &\approx C_{3\theta}(\beta g_i\langle\theta^2\rangle). \end{aligned} \tag{45}$$

Here we will be verify their observation using the present DNS data.

In figure 7, the slow-term model is tested against the pressure temperature-gradient correlation and the temperature pressure-gradient correlation evaluated from DNS data. Result for the only non-zero, z, component is shown. Clearly the model reproduces the behavior of the temperature pressure-gradient data very well throughout the domain of comparison including the near wall regions. The optimum value of the coefficient is found to be $C_{1\theta} = 2.3$. In figure 8, similar comparison is performed with the fast term model. In the interior of the flow, the DNS data shows that the correlations are nearly constant at their respective values. The fast-term model also exhibits nearly flat behavior. Depending upon the value of the model coefficient chosen, either of the correlation is reproduced well. The optimum value for matching the pressure temperature-gradient correlation is $C_{3\theta} = 0.22$ and that for temperature pressure-gradient correlation is $C_{3\theta} = 0.44$. The near-wall agreement in the fast-term case is not as good as in the slow-term case.

Dissipation of turbulent thermal flux. The model for dissipation of thermal flux is given in Section 2 and is repeated here for convenience:

$$\varepsilon_{i\theta} = f_{\varepsilon\theta}\sqrt{\varepsilon\varepsilon_\theta}F_i, \tag{46}$$

where $f_{\varepsilon\theta}$ goes to zero in sufficiently high Reynolds number flows. The dissipation of thermal flux should be identically zero in high Reynolds number turbulence when the small scales are statistically isotropic. But in a flow such as the present one, the Reynolds number is not high enough for $\varepsilon_{i\theta}$ to vanish. The dissipation $\varepsilon_{3\theta}$ calculated from DNS data is presented in figure 9. It has its highest value near the wall and is fairly low in the center of the flow. Near the walls the turbulence is least isotropic had hence the value of this dissipation is high. Away from the wall, the flow is more isotropic leading to lower values of $\varepsilon_{3\theta}$. The value of the model coefficient can be estimated from the DNS data as:

$$f_{\varepsilon\theta} = \frac{1}{F_3}\frac{\varepsilon_{3\theta}}{\sqrt{\varepsilon\varepsilon_\theta}}. \tag{47}$$

The value of $f_{\varepsilon\theta}$ thus calculated is plotted in figure 9. The coefficient appears to be a fairly strong function of z close to the walls, but is nearly a constant at 0.7 near the center of the flow.

Turbulent transport of F_i. The turbulent transport of F_i can be inferred from equation (21):

$$\mathcal{D}^F_{i\theta} = \tau[\frac{\mathcal{D}_{i\theta}}{\sqrt{K\langle\theta^2\rangle}} - \frac{1}{2}F_i(\frac{\mathcal{D}_K}{K} + \frac{\mathcal{D}_\theta}{\langle\theta^2\rangle})]. \tag{48}$$

The standard assumption is that $\mathcal{D}_{i\theta}$ can be modeled as

$$\mathcal{D}_{i\theta} \approx -\frac{1}{2}\langle u_i\theta\rangle[\frac{\mathcal{D}_K}{K} + \frac{\mathcal{D}_\theta}{\langle\theta^2\rangle}] \tag{49}$$

so that $\mathcal{D}^F_{i\theta}$ can be neglected.

The validity of this assumption is verified in figure 10, where $\mathcal{D}_{3\theta}$ and $\frac{1}{2}\langle u_3\theta\rangle[\frac{\mathcal{D}_k}{K} + \frac{\mathcal{D}_\theta}{\langle\theta^2\rangle}]$ are plotted using DNS data. First we plot $\mathcal{D}_{3\theta}$ as defined in equation (6) which is consistent with with the interpretation of $\phi_{3\theta}$ as the pressure temperature-gradient correlation (equation 44). Also plotted in this figure is $\mathcal{D}_{3\theta}$ computed without the pressure-temperature correlation (see equation 6) and this

formulation is consistent with the interpretation of $\phi_{3\theta}$ as the temperature pressure-gradient correlation (equation 45). The model appears to qualitatively capture the features well in either case but quantitative agreement is only reasonable. The overall agreement seems somewhat better with the inclusion of pressure-temperature correlation in the definition of $\mathcal{D}_{3\theta}$, as it appears in equation 6.

Budget of F_i evolution equation. Since the turbulence is statistically stationary, the evolution equation of F_i can be rewritten as (see equation 21)

$$P^F_{i\theta} + \varepsilon^F_{i\theta} + \phi^F_{i\theta} + \mathcal{D}^F_{i\theta} = 0. \tag{50}$$

The production, dissipation, pressure-strain redistribution and turbulent transport of F_i groupings can be surmised from equation (21). The z component of these quantities are shown in figure 11. The production, dissipation and pressure correlation terms are clearly larger than the transport term. Nonetheless, the transport term is not negligible, especially close to the walls.

Due to the overall reasonable predictions of the pressure-temperature correlation models and somewhat diminished size of turbulent transport in the center regions of the flow, the algebraic model may be more appropriate for the thermal flux than for the Reynolds stresses. The algebraic model for F_3 derived in Section 2 is compared against DNS data in figure 12. The model displays a bi-modal behavior not seen in the DNS data. The maximum disagreement region here coincides with the rather large disagreement region in figure 7 between the fast-pressure model and corresponding DNS data. Despite this disagreement, due to fundamental validity of the algebraic assumption in the case of F_i, we believe that a reasonable algebraic model is quite possible for F_i. The search for a better algebraic model, however, should start with the development of better pressure-gradient temperature correlation models.

5 Conclusion

The various turbulent process of second order closure modeling interest in a buoyancy driven turbulence are closely examined using direct numerical simulations data of Rayleigh Bernard convection. This flow

was selected for the investigation since it offers a unique situation where buoyant turbulence can be studied without the complicating influence of shear turbulence.

Our study demonstrates that the commonly used pressure strain correlation models perform somewhat poorly even in the interior parts of the flow away from the wall effects. While the prediction of the rapid part of the pressure strain correlation can be improved with the addition of an extended term, the ability to predict the slow pressure strain correlation remains a challenge. Turbulent transport appears to play an important part in the evolution of Reynolds stress anisotropy, and, consequently, the algebraic stress modeling assumptions are not well satisfied by this flow.

On the thermal flux modeling side, our study reaffirms the observation of Dol *et al* [2] who state that the current models capture the behavior of pressure-gradient temperature correlation rather than the pressure temperature-gradient correlation. This would obviate the current practice of splitting the pressure correlation term into homogeneous and inhomogeneous parts. The data shows that the thermal flux dissipation is not negligible and that the model coefficient in nearly a constant away from the walls. The turbulent transport appears to play a somewhat smaller, but still significant role in the evolution of thermal flux. Overall, the likelihood of a reasonable algebraic model appears more promising in the case of thermal flux, but the development of such a model can only come from improved pressure-correlation models.

Fully-explicit and self-consistent algebraic models for the Reynolds stress and thermal flux have also been derived from their respective evolution equations using the weak-equilibrium assumption. Although not quite applicable for the present flow, we expect these models to be adequate for realistic flows at higher Reynolds numbers where the assumptions made are likely to be more valid.

Acknowledgements. SB was also partly supported by the Division of Mathematical Sciences (NSF DMS 96-22889) of National Science Foundation.

References

[1] K. Hanjalic, *Achievements and limitations in modeling and computation of buoyant turbulent flows and heat transfer.* Proc. 10th Int. Heat Transfer Conf., Brighton, UK, 1993.

[2] H. S. Dol, K. Hanjalic and S. Kenjeres, *A comparative assessment of the second-moment differential and algebraic models in turbulent natural convection.* Submitted to the Int. J. Heat and Fluid Flow (May 1996).

[3] S. S. Girimaji and K. Hanjalic, *Fully-explicit algebraic model for thermal flux in buoyant flow.* Manuscript under preparation.

[4] R. Boudjemadi, V. Maupu, D. Laurence and P. Le Quere, *Budgets of turbulent stresses and fluxes in a vertical slot natural convection flow at Rayleigh* $Ra = 10^5$ *and* $5.4\ 10^5$, Eng. Foundation 'Turbulent heat transfer' Conference, San Diego, March 1996.

[5] T. A. M. Versteegh, F. T. M. Nieuwstadt and A. A. van Steenhoven, *Private Communication*, Delft University of Technology, The Netherlands (1996).

[6] T. W. J. Peeters and R. A. W. M. Henkes, *The Reynolds stress model of turbulence applied to the natural convection boundary layer along a heated vertical plate,* Int. J. Heat Mass Transfer, **35**, 2, 403-420, 1992.

[7] S. Balachandar, M.R. Maxey and L. Sirovich, *Numerical simulation of high Rayleigh number convection,* J. Sci. Comput., **4**, 219-236, 1989.

[8] S. Balachandar, *Structure of turbulent thermal convection*, Phys. Fluids. A, **4**, 2715-2726, 1992.

[9] B. Castaing, G. Gunaratine, F. Heslot, L. Kadanoff, A. Libchaber, S. Thomas, X. Z. Wu, S. Zaleski and G. Zannetti, *Scaling of hard thermal turbulence in Rayleigh-Benard convection*, J. Fluid Mech., **204**, 1, 1989.

[10] I. H. Tarman, *Analysis of turbulent thermal convection*, PhD Thesis, Brown University, Providence, RI, 1989.

[11] J. R. Ristorcelli, J. L. Lumley, and R. A. Abid, *A rapid-pressure covariance representation consistent with the Taylor-Proudman theorem materially frame indifferent in the two-dimensional limit*, J. Fluid Mech., **222**, 111 - 152, 1995.

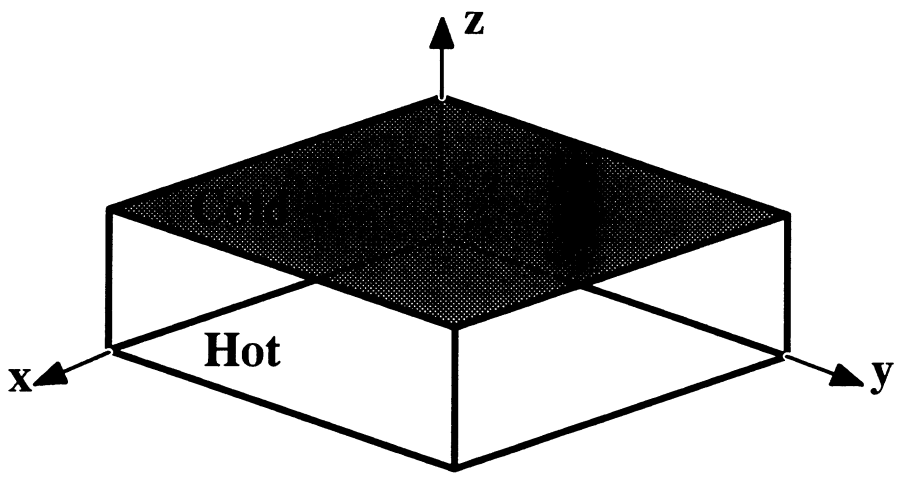

Figure 1: Schematic of the computational model of Rayleigh-Benard convection.

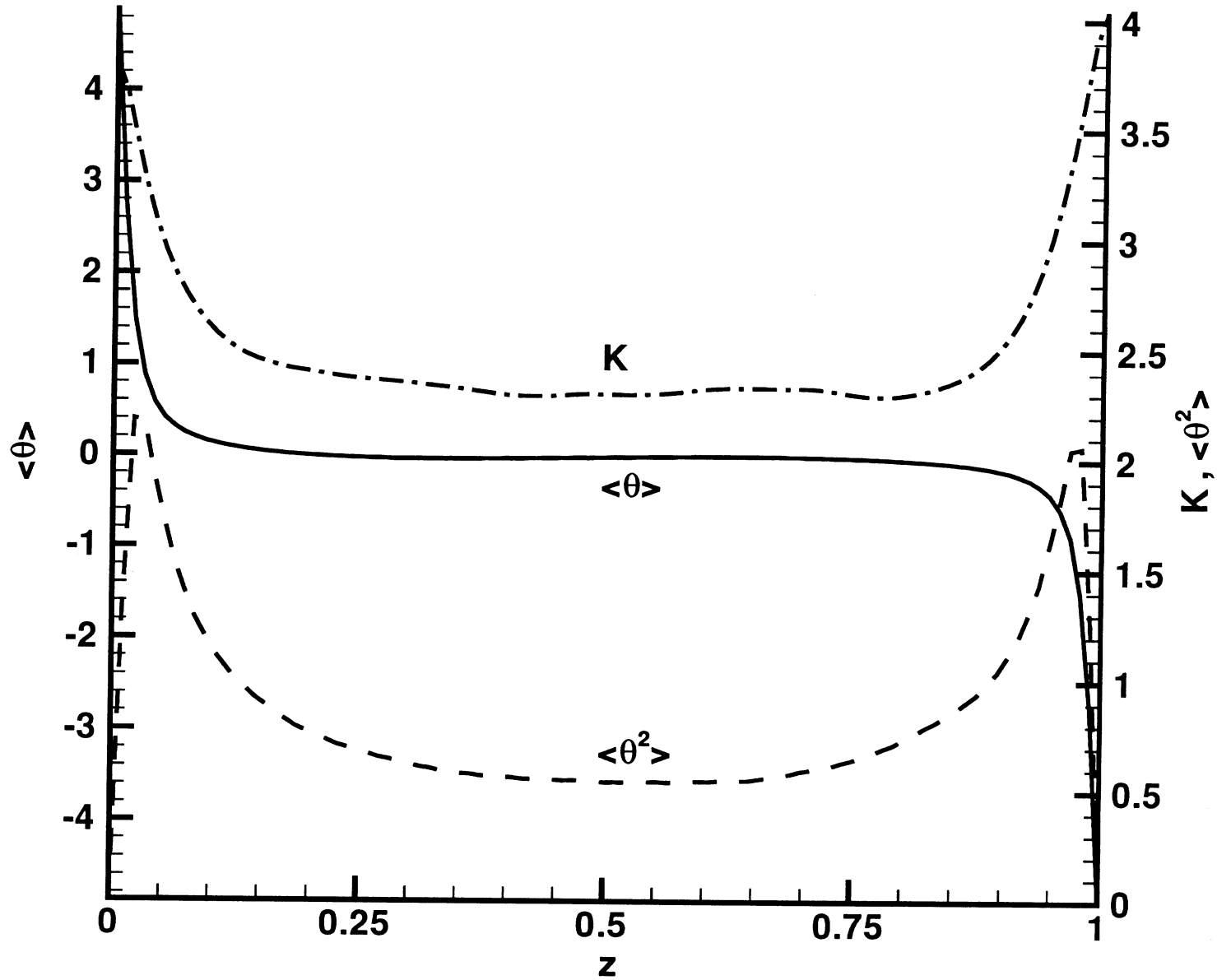

Figure 2: Variation in the mean temperature, $< \theta >$, mean square temperature fluctuation, $< \theta^2 >$ and turbulent kinetic energy, K in the vertical direction.

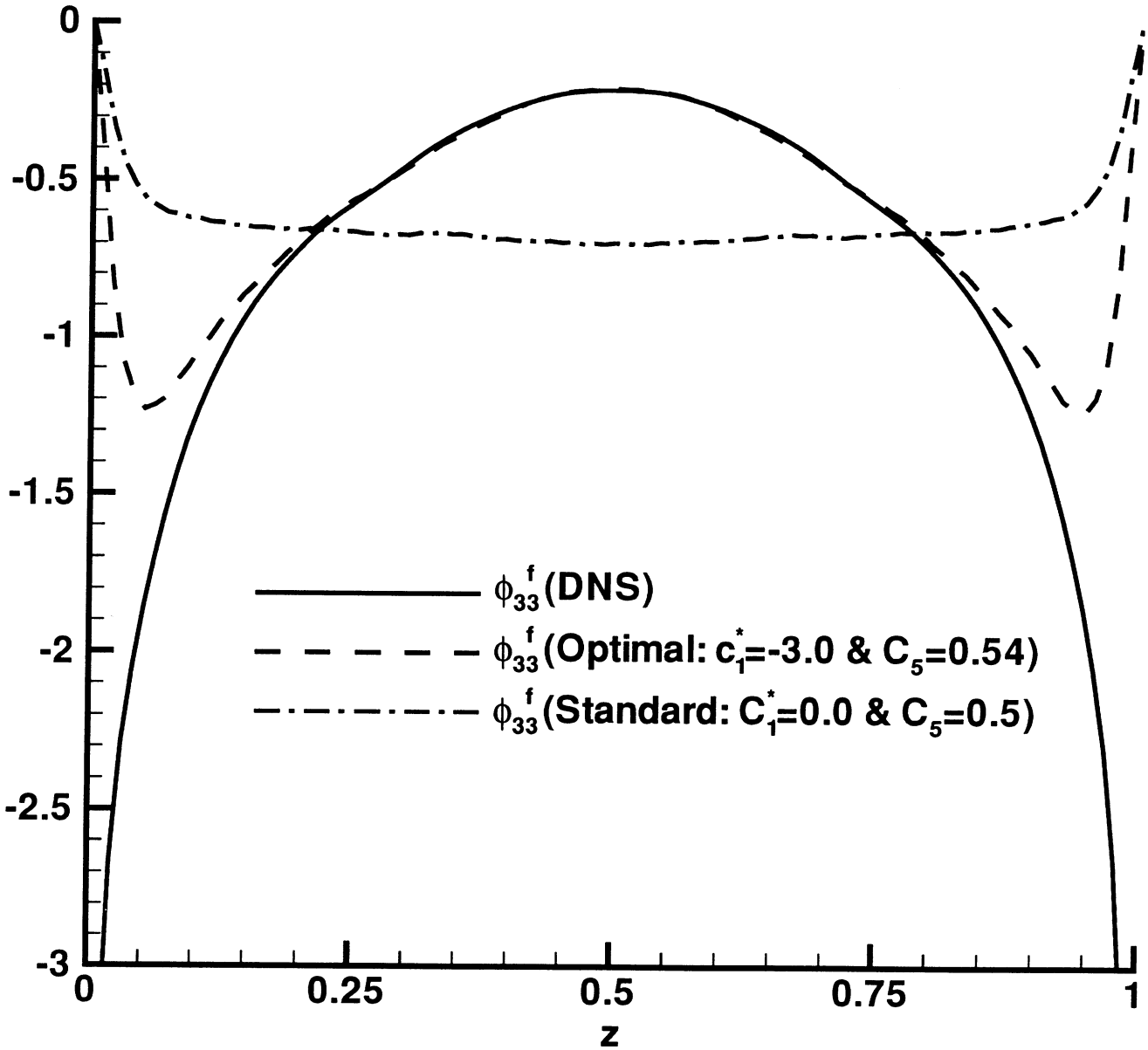

Figure 3: Pressure-strain correlation fast term: DNS data vs. model. Both a standard model with $C_1^2 = 0.0$ and $C_5 = 0.5$ and an optimal model with $C_1^2 = -3.0$ and $C_5 = 0.54$ are compared with the DNS data. The optimal value for the constants are evaluated by minimizing the difference between the model and the DNS data over the interior 50% of the layer.

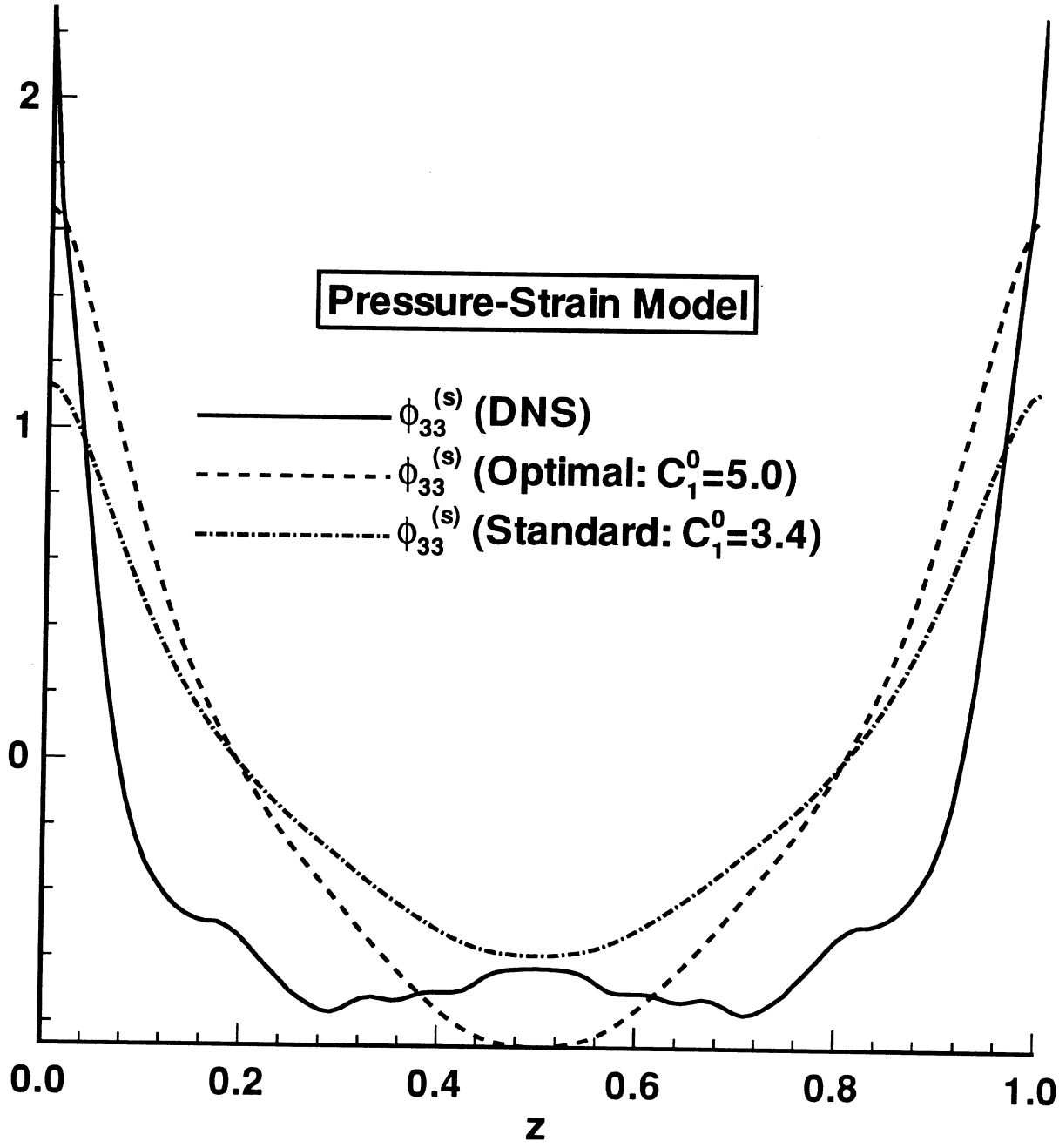

Figure 4: Pressure-strain correlation slow term: DNS data vs. model. Here again the results of both the standard and optimal pressure-strain model are compared with the DNS data.

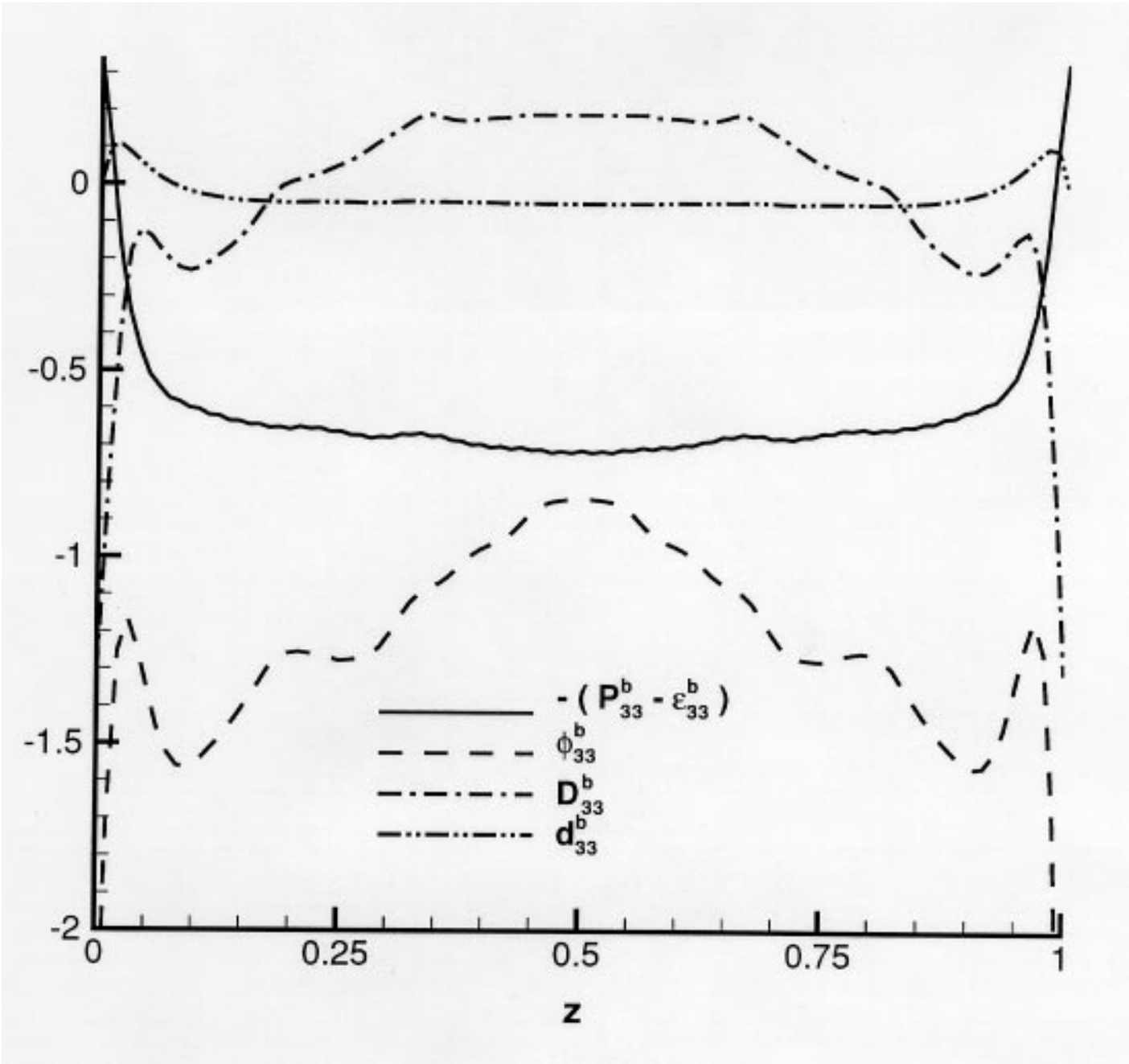

Figure 5: Budget of b_{ij} evolution equation.

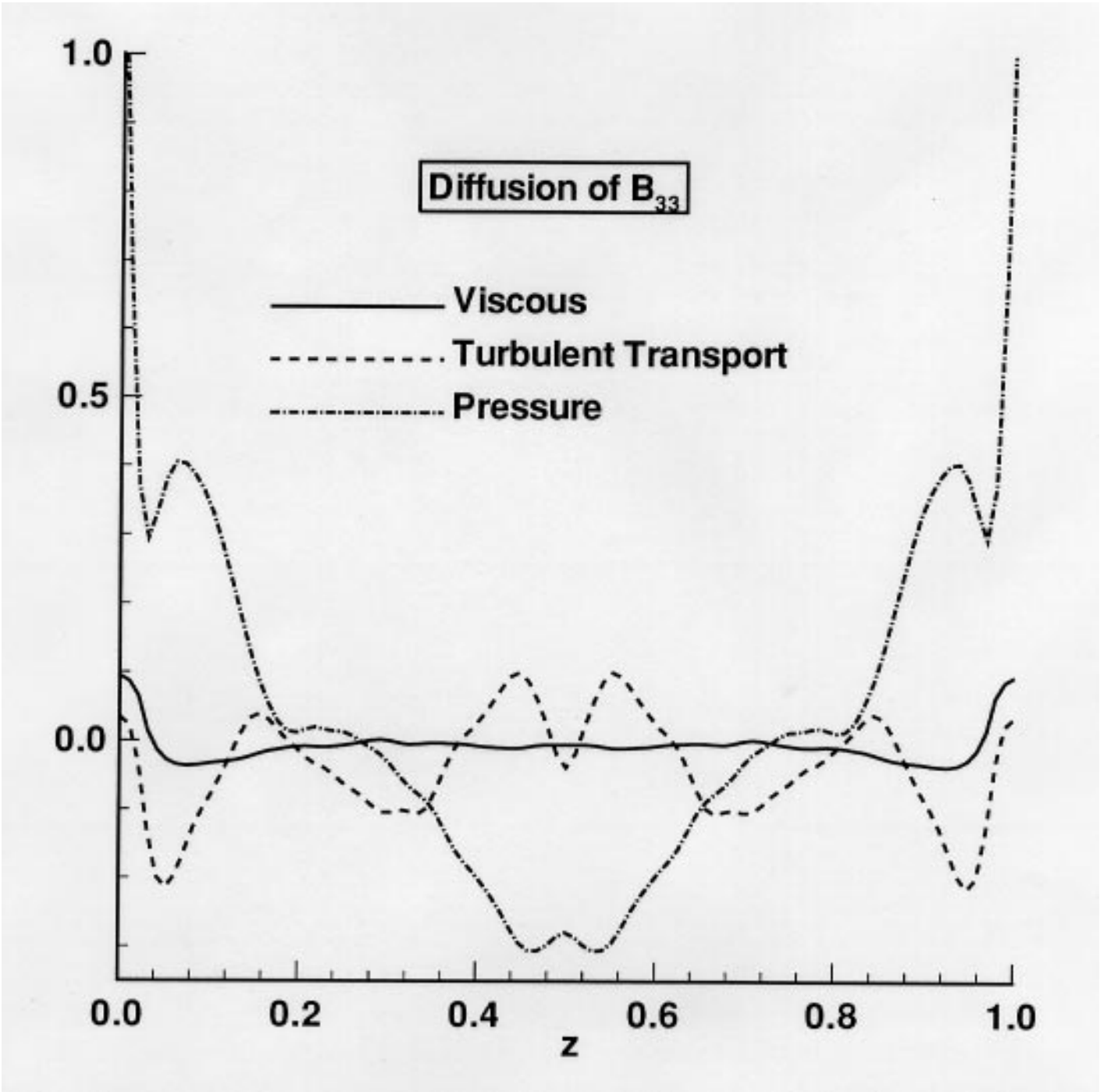

Figure 6: Components of turbulent transport of b_{ij}.

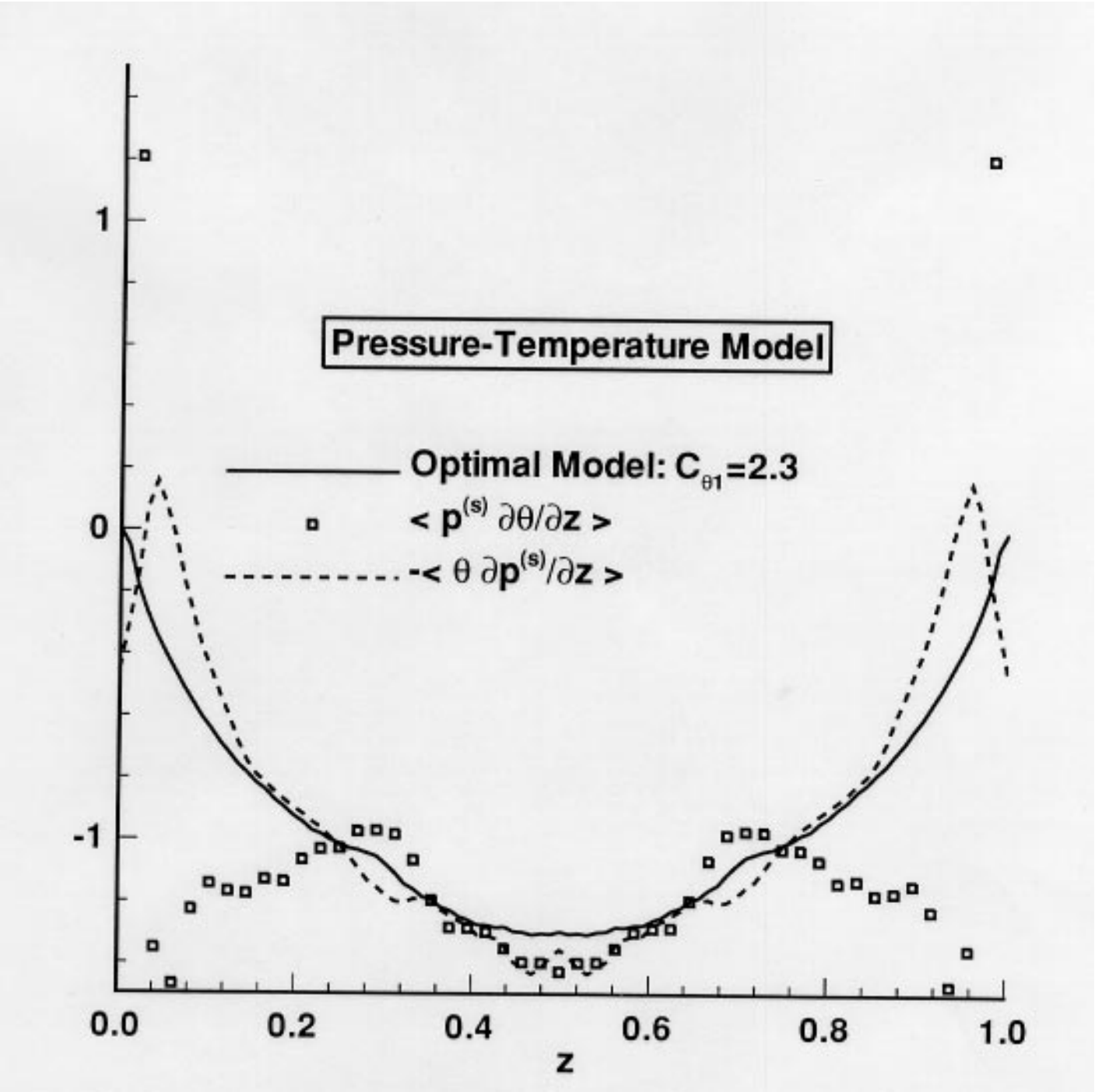

Figure 7: Pressure-temperature correlation for the slow term. DNS data vs. model. The DNS data for both the pressure-temperature gradient and the temperature-pressure gradient terms are shown.

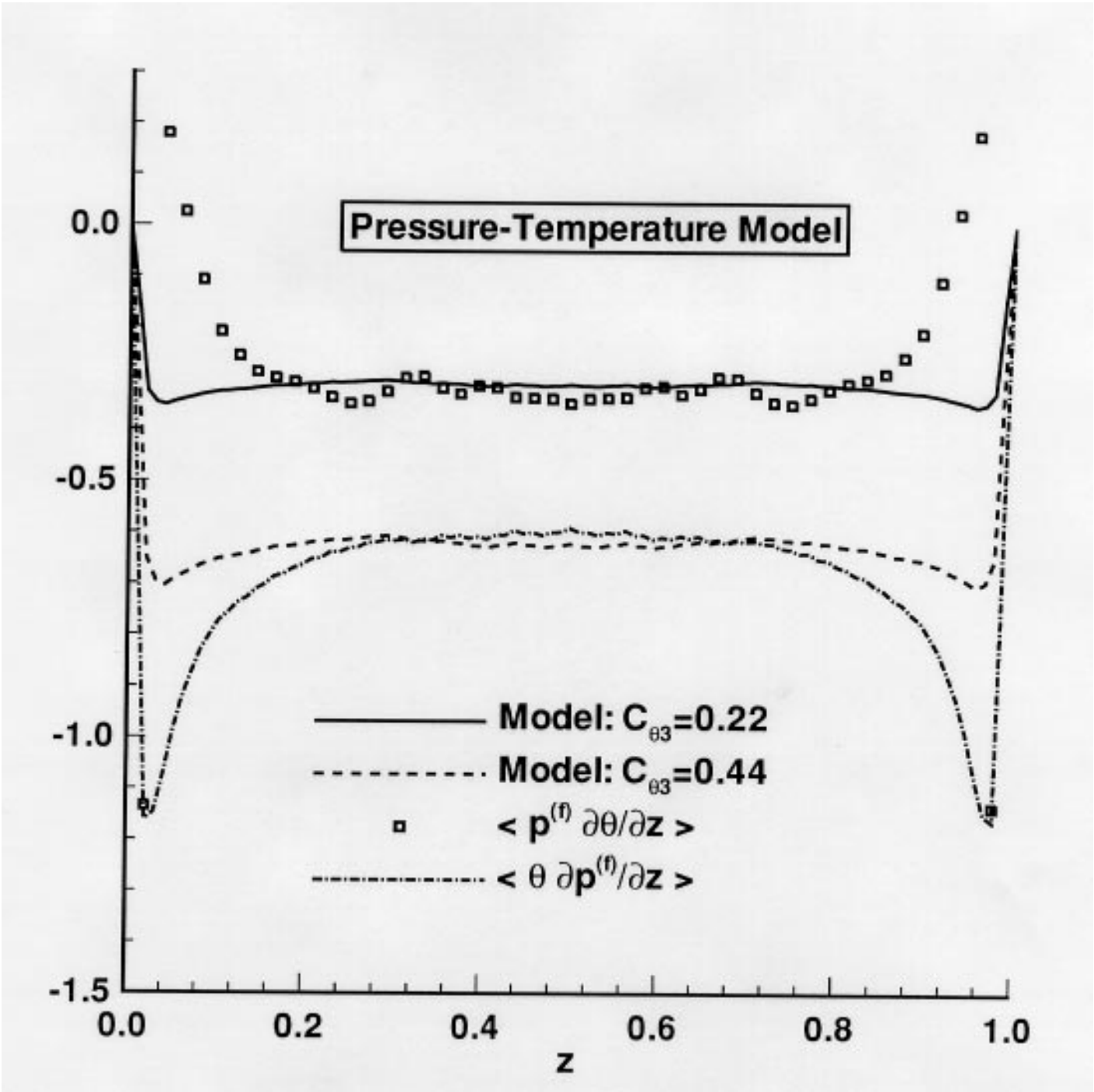

Figure 8: Pressure-temperature correlation for the fast term. DNS data vs. model. The DNS data for both the pressure-temperature gradient and the temperature-pressure gradient terms are shown.

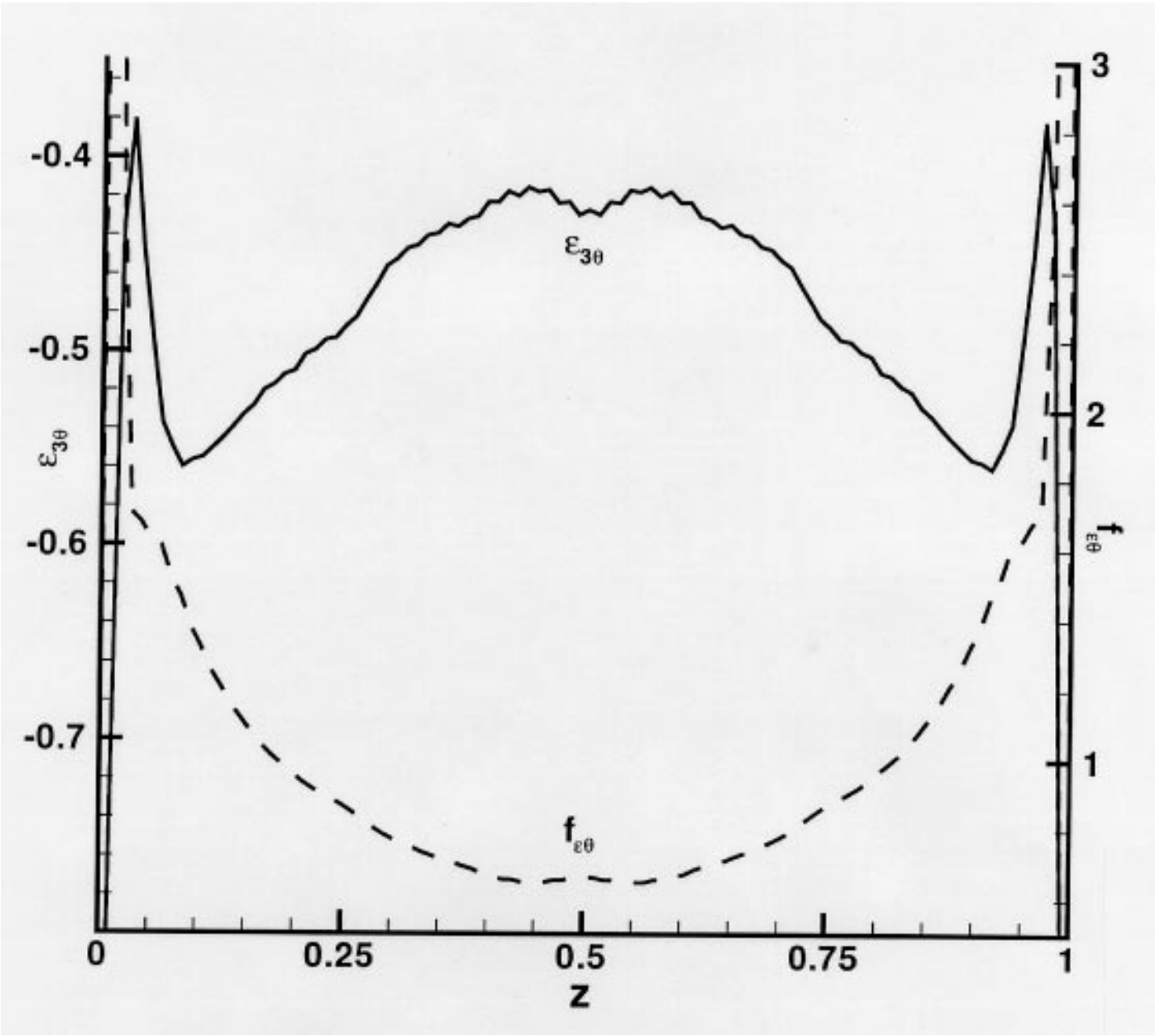

Figure 9: A plot of dissipation of turbulent thermal flux, $\varepsilon_{i\theta}$ against z. Also shown is the model constant, $f_{\varepsilon\theta}$ evaluated from the DNS data.

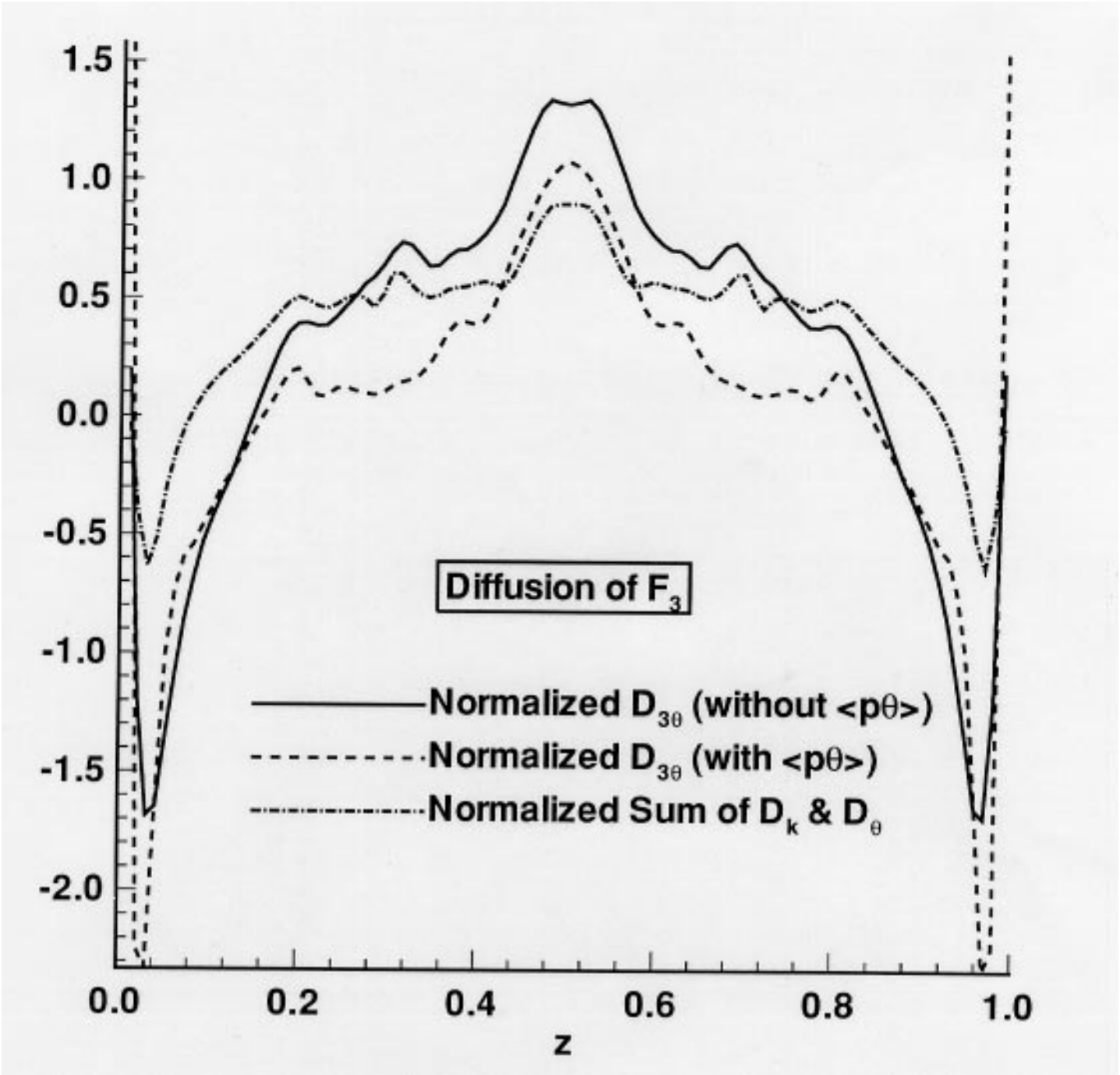

Figure 10: Turbulent transport of F_i.

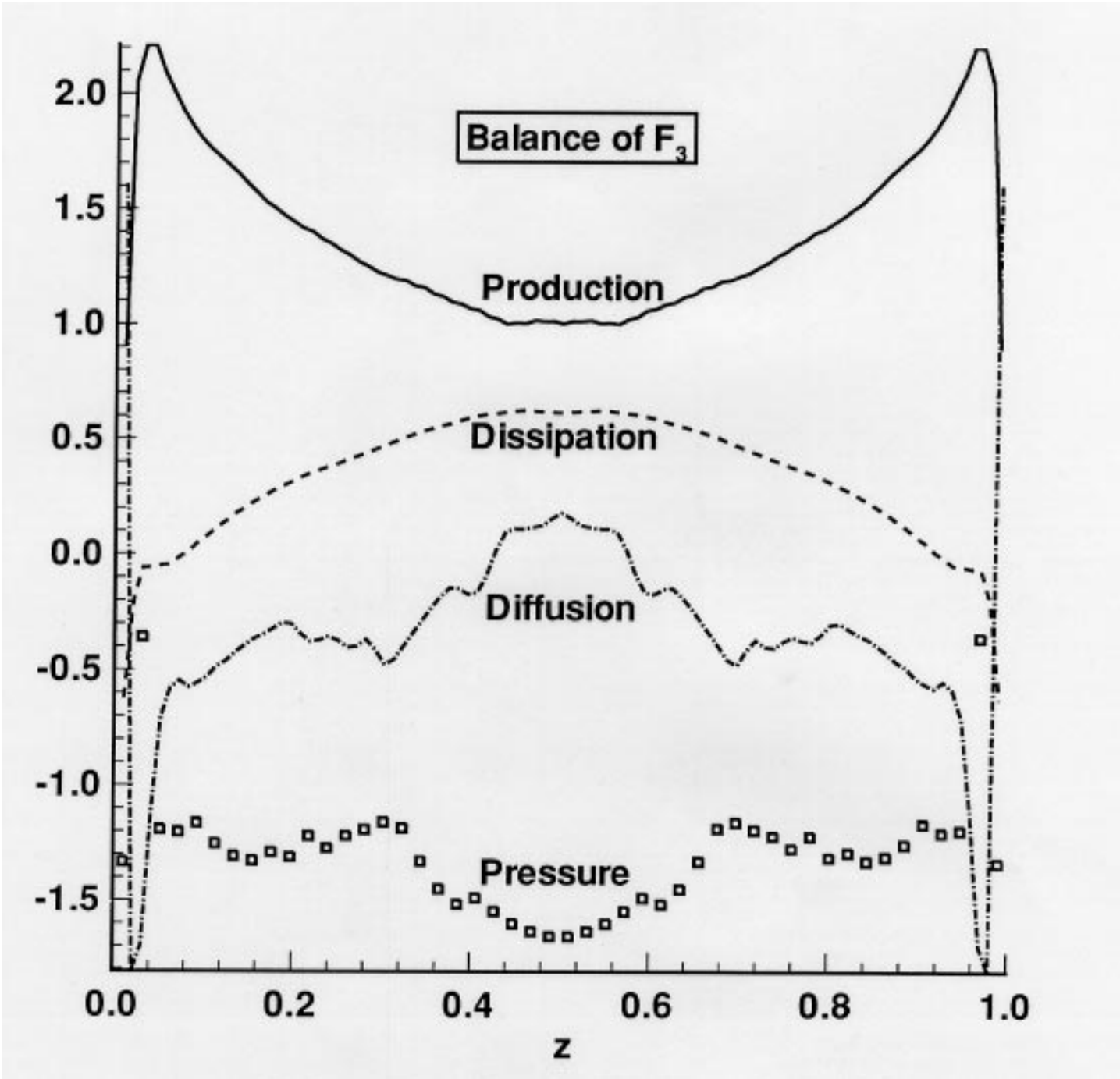

Figure 11: Budget of F_i evolution equation.

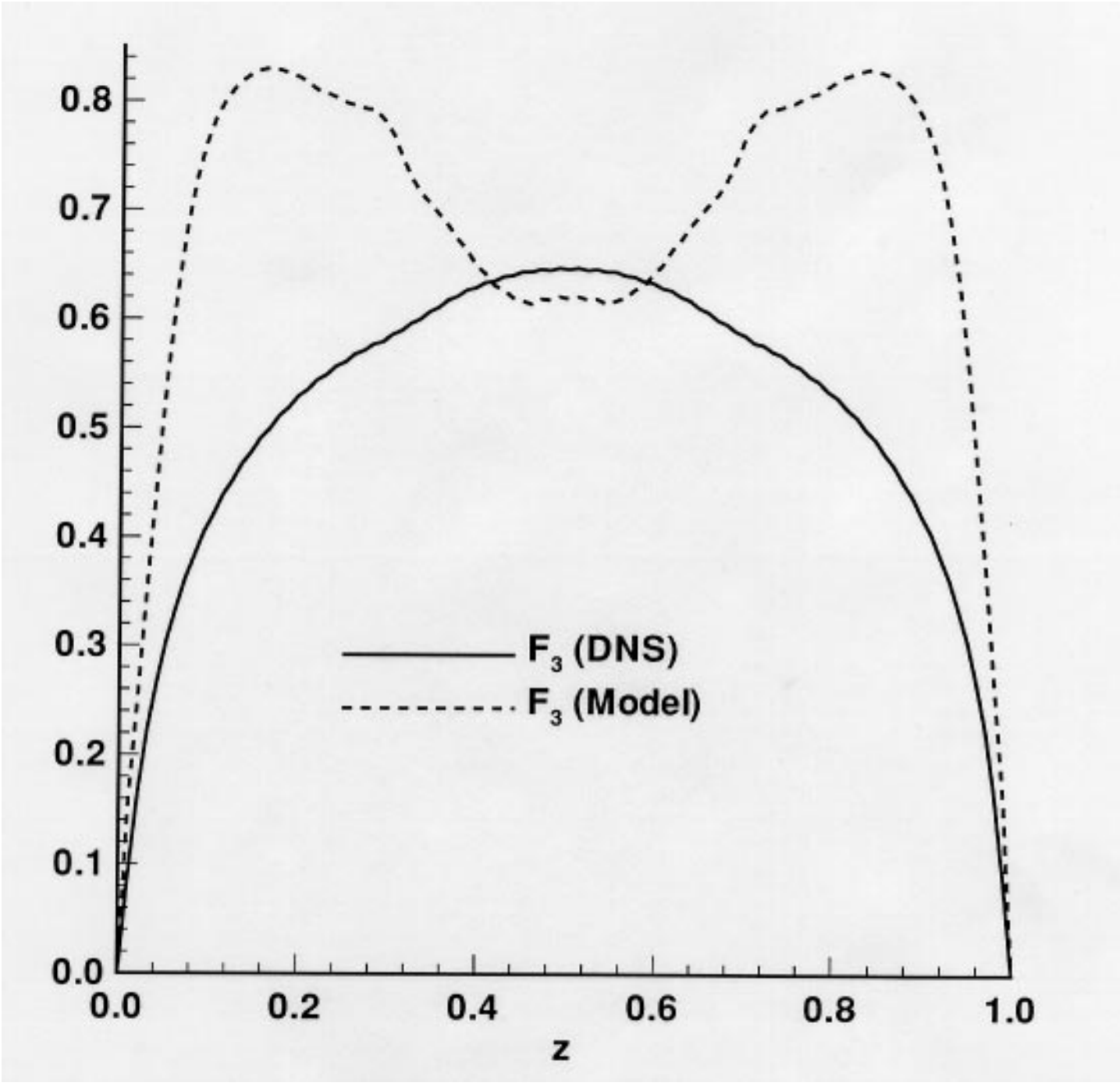

Figure 12: Algebraic model for F_3.